International Journal of Coal Science & Technology (2023) 10:53
https://doi.org/10.1007/s40789-023-00610-8

RESEARCH

Extraction and identification of spectrum characteristics of coal and rock hydraulic fracturing and uniaxial compression signals

Ya'nan Qian[1,2] · Quangui Li[1,2,3] · Qianting Hu[1,2] · Zhizhong Jiang[4] · Ronghui Liu[1,2] · Jie Li[1,2,5] · Wenxi Li[1,2] · Changjun Yu[1,2]

Received: 5 April 2023 / Revised: 29 May 2023 / Accepted: 18 July 2023

Abstract

Microseismic (MS) events generated during coal and rock hydraulic fracturing (HF) include wet events caused by fracturing fluid injection, in addition to dry events caused by stress perturbations. The mixture of these two events makes effective fracturing MS events pickup difficult. This study is based on physical experiments of different coal and rock HF and uniaxial compression. The differences of waveform characteristic parameters of various coal and rock ruptures were analyzed using the Hilbert–Huang transform, leading to some useful conclusions. The phase characteristics of the acoustic emission (AE) energy differed significantly and responded well to the pumping pressure curve. The AE waveforms of HF exhibit similar energy and frequency distribution characteristics after Empirical mode decomposition. The main frequency bands for coal, sandstone, and shale samples are 100–300 kHz, while the mudstone sample is in the range of 50–150 kHz. The decay ratios for coal, sandstone, shale and mudstone samples are 0.78, 0.83, 0.67 and 0.85, respectively. When compared to the uniaxial compression test, the main frequency bands of HF were reduced for coal, sandstone and mudstone samples, whereas shale remained essentially unchanged. The duration, instantaneous energy, and total energy of the HF waveform are smaller than those of uniaxial compression, while the decay ratio is greater, especially for the mudstone samples. The waveform characteristic parameters, trained using the multilayer perceptron neural network, can effectively identify HF and uniaxial compression events with an accuracy of 96%.

Keywords Hydraulic fracturing · Uniaxial compression · Hilbert–Huang transform · Acoustic emission · Microseismic

1 Introduction

Hydraulic fracturing (HF) technology has been proved to be an effective method for preventing coal and rock dynamic disasters in coal mines (Li et al. 2015). Microseismic (MS)/acoustic emission (AE) monitoring technology is a geophysical real-time monitoring technology used to explain the rupture behavior of coal and rock by analyzing MS/AE signals (Jiang et al. 2020; Li et al. 2021a, b). Identifying and picking up effective HF events is essential when using MS monitoring techniques to explain HF behavior. However, MS events generated during coal and rock HF include wet events caused by fracturing fluid injection in addition to dry events caused by stress perturbations. Meanwhile, the simultaneous fracturing of multiple lithologies in the top and bottom of the coal seam makes the identification and picking up of effective signals more complex. The acoustic emission (AE) waveforms of coal and rock cracks contain a wealth of information about the physical and mechanical

✉ Quangui Li
liqg@cqu.edu.cn

1 State Key Laboratory of Coal Mine Disaster Dynamics and Control, Chongqing University, Chongqing 400044, China

2 School of Resources and Safety Engineering, Chongqing University, Chongqing 400044, China

3 State Key Laboratory of Mining Response and Disaster Prevention and Control in Deep Coal Mines (Anhui University of Science and Technology), Huainan 232001, China

4 Mining College of Guizhou University, Guiyang 550025, Guizhou, China

5 China Coal Technology and Engineering Group Shenyang Research Institute, Fushun 113122, China

Published online: 26 September 2023

properties and rupture patterns, and only an effective time–frequency analysis method can extract the waveform features accurately(Kong et al. 2016; Li et al. 2019; Moriya et al. 2006).

As we know, the biggest difference between fracturing fluids and stress disturbance-induced hydraulic fracturing events is the involvement of water. Water intervention affects the characteristics and propagation pattern of the MS signals, such as the attenuation of energy and dispersion of the signal (Mueller et al. 2010; Stanchits et al. 2015). Therefore, MS events generated by the HF of coal seams can also differ from conventional ruptures in terms of generation mechanisms and signal characteristics. In order to identify and pick up effective HF events, it is necessary to understand the characteristics of MS signals under different fracture modes.

Previous research based on the HF of coal and rocks has focused on the damage mechanisms, crack extension mechanisms, stress evolution (Wang et al. 2021), and MS position (Jiang et al. 2019; Li et al. 2021b, a). The characteristics of AE signals form the basis for studying coal and rock rupture patterns (Zhang et al. 2019a, b, c). Different rock conditions, stress conditions, and stress-loading methods may produce different AE signal characteristics. The main time–frequency analysis methods include wavelet transform (WT) (Liang et al. 2020; Zhang et al. 2019a, b, c), S-transform (Xiao et al. 2018), Wigner–Ville distribution (WVD), Choi-Williams distribution (CWD), and Hilbert–Huang transform (HHT) (Li et al. 2016a, b; Zhang et al. 2016). In contrast to the Fourier transform, the HHT not only reflects the overall frequency component of the signal but also provides a characteristic of the change in frequency over time. In contrast to the WT, the HHT is free from the limitation of relying on the Fourier transform. HHT does not require a stable signal within the window and does not depend on the choice of a priori wavelet bases (Li et al. 2012, 2020). As a result, the HHT is less prone to bias and is particularly advantageous for MS signals, which are typically non-smooth and non-linear.

Researchers have conducted extensive investigations on HF using MS/AE technologies. By analyzing different fracturing and acoustic parameters, the process of crack extension by HF was indirectly revealed (Li et al. 2018). The response characteristics of coal subjected to HF were investigated by real-time monitoring of the borehole strain and AE (Liang et al. 2017). The crack distribution in the HF was studied using the MS location method (Li et al. 2022). The characteristics of the AE waveform parameters were investigated to evaluate the effectiveness of HF and to optimize HF strategies in coal seams (Yue et al. 2019). Joint studies were also conducted on crack networks for HF in relation to other geophysical research directions (Niemz et al. 2021; Zhang et al. 2019a, b, c; Zou et al. 2016). Further, the effect of injected fluid viscosity on crack extensions by HF was studied, and the softening effect of saturated fluids on rocks was determined (Damani et al. 2018).

HF differs from other mining MS activities in that water intervention can affect coal strength, stress distribution and crack extension to varying degrees. Therefore, the effect of water cannot be ignored when distinguishing MS signals caused by fracturing fluids and stress perturbations. Considering that HF will inevitably cause the simultaneous fracturing of the top and bottom coal seam, the test platform for coal and rock HF and uniaxial compression was designed and built in this study. The AE waveform characteristics of coal and rock under different rupture modes were analyzed by HHT, and different AE signals were identified by multilayer perceptron (MLP) neural network. This study is a fundamental work in explaining HF behaviors using MS monitoring technology, which is important for identifying and picking up effective HF events.

2 Experiments

2.1 Experimental conditions

The uniaxial compression and HF test systems for coal and rock are shown in Fig. 1. Four different lithologies (coal, sandstone, shale, and mudstone) from the coal strata were selected for this experiment. Figure 1a shows the prepared square and cylindrical samples. The samples for the uniaxial compression tests were machined into standard cylindrical samples (Φ50 mm × 100 mm) according to the International Society for Rock Mechanics (ISRM). The ends and sides of the samples were carefully ground such that non-parallelism and non-perpendicularity were less than 0.02 mm. All samples were in a naturally watery state and were not subjected to any drying process. The samples were numbered A1, A2, A3, B1, B2, B3, C1, C2, C3, D1, D2, and D3, respectively.

The samples for the HF tests were processed into squares and two samples were prepared for each lithology with dimensions of 100 mm × 100 mm × 100 mm, numbered E1, E2, F1, F2, G1, G2, H1, and H2, respectively. When prefabricated fracture holes for samples, in order to avoid excessive damage to the interior of the sample, first fix the sample on the cutting frame, select a sharp cutting tool to cut the sample, and promptly clean up the cutting debris to ensure smooth cutting without excessive damage to the sample. The parameters of samples preparation are shown in Table 1.

Figure 1b shows the uniaxial compression test system, Fig. 1c shows the HF test system, and Fig. 1d shows the AE monitoring system. These three parameters of the peak definition time, hit definition time, and hit lockout time must be changed according to the actual waveform, and a segmented approach is recommended. The preamp gain range is 40 dB, the frequency range of the AE sensor is 50–400 kHz,

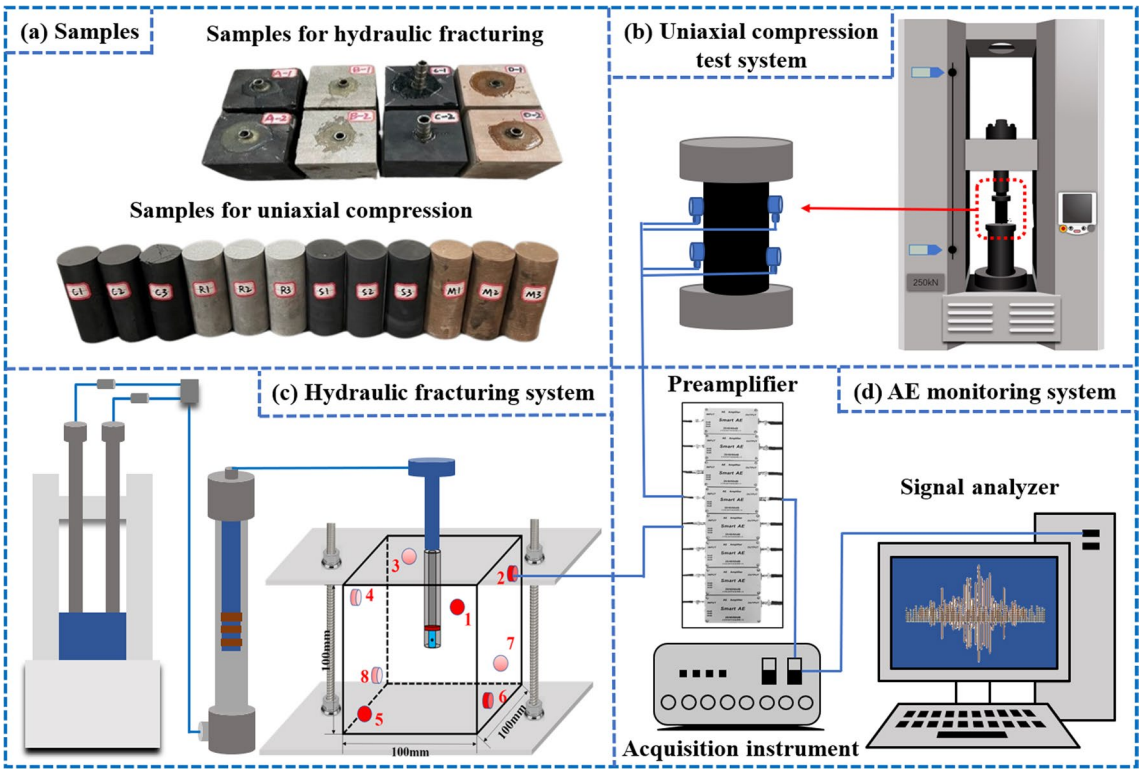

Fig. 1 Schematic of the experimental system. **a** Samples **b** Uniaxial compression test system **c** HF system **d** AE monitoring system

Table 1 Parameters of samples preparation

Drilling depth (mm)	Drilling diameter (mm)	Fracture pipe inner diameter (mm)	Fracture pipe outside diameter (mm)	Sealing depth (mm)	Epoxy resin ratio	Sample drying time (h)
40	20	8	15	45	1:1	24

the threshold value is 40 dB, and the sampling frequency is 3 MHz.

2.2 Experimental methods

Firstly, uniaxial compression tests were performed on coal and rock samples. The loading rate of uniaxial compression is 0.1 mm/min. The test results showed that the average uniaxial compressive strength (UCS) of coal, sandstone, shale and mudstone were 14.21, 82.40, 114.52, and 35.72 MPa, respectively. The elastic modulus is 3.30, 12.40, 9.02, and 7.30 GPa, respectively. The coal samples had the lowest compressive strength, and the shale samples had the highest compressive strength.

Secondly, HF tests were performed on coal and rock samples. After the AE monitoring system and HF system were installed, their stability and gas tightness were tested separately. Then the pump pressure system is turned on and the test is performed by controlling the flow rate of fracturing fluid. The AE signal and pressure curves data are collected separately, and the end of the test is signaled when the fracturing fluid breaks through the surface of the samples. Finally, close the valve and store the data.

3 Results

3.1 AE Energy characteristics of HF waveforms

AE signal is the phenomenon of elastic wave propagation due to damage or rupture of coal and rock samples. AE energy is an important parameter to describe the severity of damage of coal and rock samples. The AE energy is usually defined as the measured area under the envelope of the AE signal. Since the AE energy is sensitive to both amplitude and duration, and less dependent on the voltage threshold and operating frequency, the energy parameter can more accurately describe the original waveform of AE. The

higher the AE energy, the greater the degree of rupture and the more serious the damage produced within the coal and rock samples. In the analysis of this paper, E1, F1, G1, and H1 were selected for analysis. The variation patterns of AE energy and cumulative energy with pumping pressure curves during HF of different coal and rock are shown in Fig. 2. Figure 2 also shows the physical diagram of the fracture of different coal and rock samples and the waveforms when the main fracture occurred. The AE waveforms at this stage can more clearly reflect the original characteristics of coal and rock fracture. Therefore, the waveforms of different coal and rock samples when the main fracture occurred during HF were extracted separately for subsequent analysis.

From Fig. 2, it can be seen that the differences in the stage characteristics of AE energy are obvious and have a high consistency with the variation pattern of pump pressure curve. At the initial stage of fracturing, the pump pressure curve increased slowly, and the AE energy was small at this stage, which was due to the need of fracturing fluid to fill the fracturing compartment at the early stage of fracturing. When the fracturing fluid filled the fracturing compartment, the pump pressure gradually increased. When the pump pressure reached the minimum strength of coal and rock samples rupture, cracks will be generated inside the coal and rock samples. At this time, the AE energy increased abruptly and the cumulative energy curve showed an obvious inflection point. Then the pump pressure curve rose slowly. When the pump pressure reached the maximum strength that the coal and rock samples can sustain, the fracturing fluid will pass through the coal and rock samples, resulting in the overall rupture of the samples. At this time, the pump pressure dropped abruptly, representing the end of the experiment. The continuous rise in pump pressure of coal sample beyond the first inflection point could be indicative of stress redistribution within the coal sample. As the hydraulic fracturing process progresses, the induced fractures may propagate and interact with existing natural fractures or stress concentration zones within the coal. Rock samples are more brittle compared to coal samples. When the pump pressure reaches the compressive strength of the rock, the resulting cracks tend to penetrate directly through the sample, resulting in a sudden decrease in pump pressure. In contrast, the coal sample, due to its large number of internal microcracks, the cracks do not penetrate the sample after the first inflection point, but regain stress equilibrium after

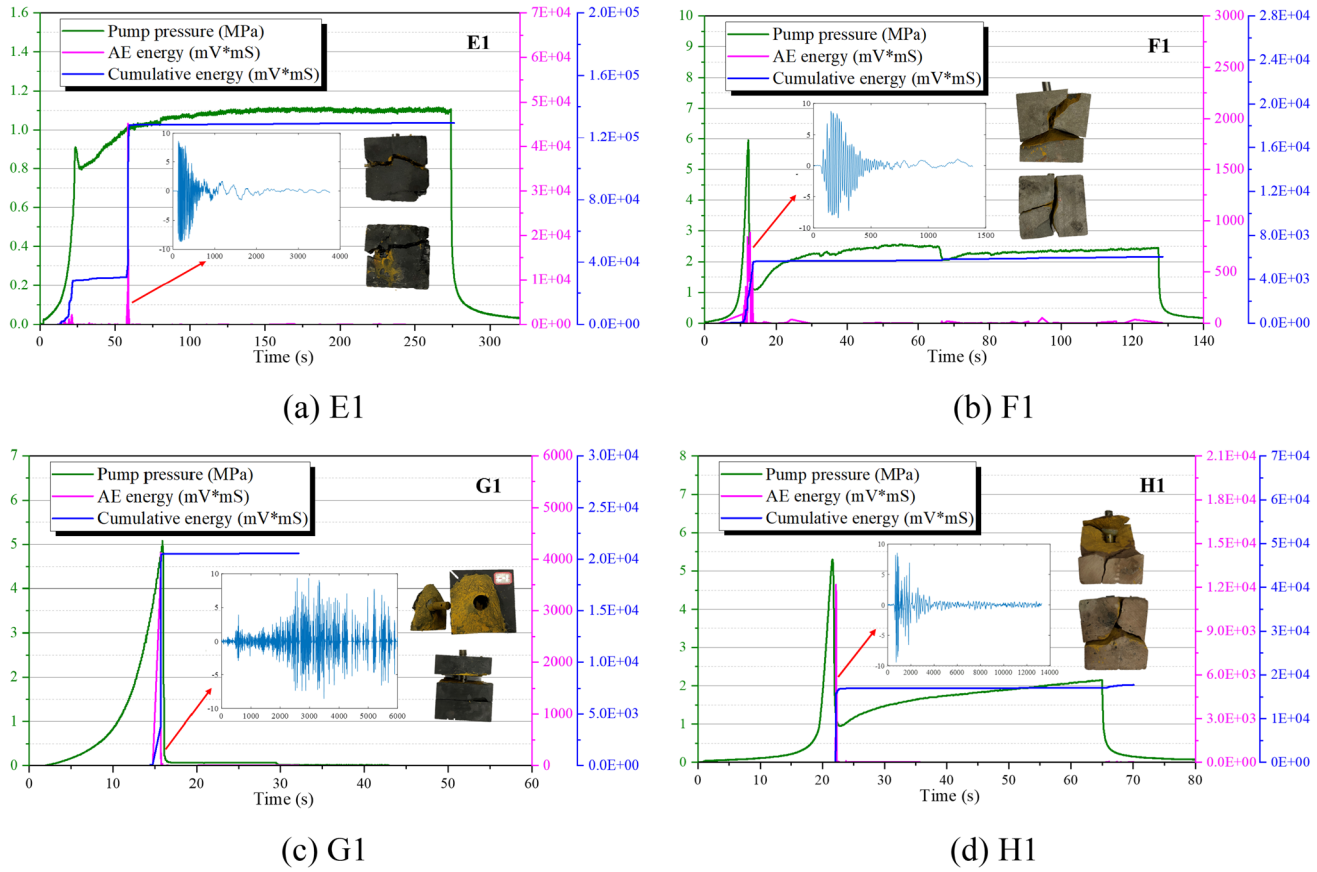

Fig. 2 Comparison of AE energy and pumping pressure curves for coal and rock during HF

penetrating with the native cracks, so the pump pressure continues to rise afterwards.

3.2 Time–frequency characteristics of HF waveforms

The frequency characteristics of the AE signal are the most representative of the motion pattern of the original waveform. Larger cracks tend to produce events with larger amplitudes and containing lower frequency components. Therefore, frequency is an important criterion to distinguish the acoustic emission signals of different lithologies and different fracture characteristics. Huang et al. (1998, 1999) proposed the empirical mode decomposition (EMD) method in 1998 and introduced the concept of Hilbert spectrum and Hilbert spectrum analysis. The National Aeronautics and Space Administration named this method the HHT. HHT analysis can obtain the frequency characteristics of the signal with time, and it is less prone to bias and more stable in dealing with nonlinear MS signals. The characteristics of a typical AE waveform within the rupture stage were analyzed based on the changes in the pressure curves and trends of the AE energy. Based on the sequence of small to large intervals between adjacent waveform peaks, EMD was used to decompose the AE waveforms of different coal and rock cracks separately. Several intrinsic mode function (IMF) components can be obtained. The EMD of AE waveforms of different coal and rock HF is shown in Fig. 3. Because EMD does not require a predetermined or mandatory basis function to be provided in advance, the characteristics of each IMF component are determined by the original waveform.

As shown in Fig. 3, all waveforms were decomposed into 6–8 IMF components in order from high to low frequencies. Among them, the IMF1 component had the highest

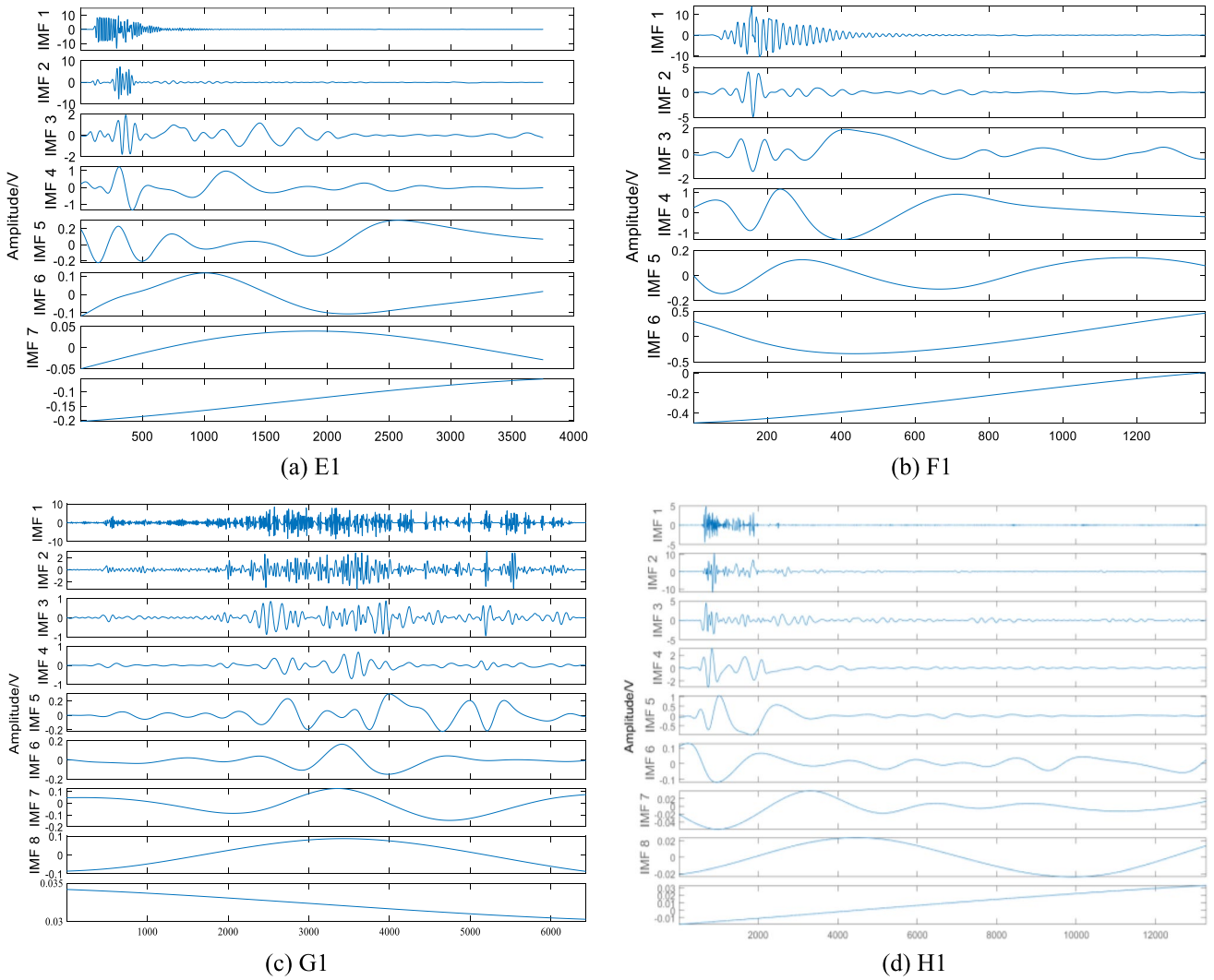

Fig. 3 EMD of the AE waveforms of different coal and rock HF

frequency and shortest fundamental wavelength. As the decomposition process proceeded, the frequency of the IMF components gradually decreased and the fundamental wavelength gradually increased. The decomposition is completed when the final residual component reaches a very low frequency. The eight sets of signals demonstrate that the average amplitude of all IMF components decreases in order, and that the main energy is focused on IMF1–IMF3. IMF1–IMF3 are the main components of high frequency and large amplitude of the original signal, and these characteristics mean that they contain most of the original energy. Therefore, this range can be defined as the dominant frequency bands for coal and rock cracks. The IMF4–IMF6 components have smaller amplitudes and frequencies. This range can be defined as the intrinsic components of the AE signals. The AE signals in this range may be caused by background noise or electrostatic interference from the loading equipment. The IMF7–IMF8 components have the smallest amplitudes and frequencies, and the IMF components in this range are the residual terms after EMD. The IMF components of this range should be zero. The amplitudes of this residual terms and its distribution represent the drift phenomenon and the extent of the AE acquisition equipment. From the analysis results, it can be seen that although the physical properties of the samples are different, the AE waveforms show similar distribution characteristics of energy and frequency after EMD.

EMD of the AE waveforms decomposes the original signal into a series of IMF components that satisfy the conditions. The Hilbert transform was then applied to the IMF components to obtain the associated characteristic parameters, such as the instantaneous frequency and Hilbert spectra of the original signal. The AE waveforms and Hilbert spectra of different coal and rock HF are shown in Fig. 4. The background noise amplitude was controlled to within 0.1 mV, indicating good contact between the sensors and the samples. The AE waveform amplitudes are much larger than the noise amplitude; therefore, the effect of background noise on the AE waveforms can be ignored. As shown in Fig. 4, there was a concentration of energy and frequency bands in the spectra of all four test samples. The main frequency bands of the coal, sandstone, and shale samples are 100–300 kHz, and the main frequency band of the mudstone sample HF is 50–150 kHz.

3.3 Three-dimensional energy spectrum characteristics of HF waveforms

The Hilbert transform is a linear transform, which emphasizes the local properties of the waveform. The instantaneous frequencies obtained from it avoid the non-existent high and low frequency components produced by Fourier transform. The energy of the original signal is distributed in a three-dimensional energy spectrum after the Hilbert transform. It is possible to visualize the distribution of AE energy on a time–frequency scale. This provides an important reference for estimating the scale of damage and amount of energy released instantaneously. The three-dimensional energy spectra of the AE waveforms from the different coal and rock HF samples are shown in Fig. 5. The color bar on the right indicates the amount of energy, where darker colors correspond to more energy.

The Hilbert three-dimensional energy spectrum clearly shows the AE waveform energy pattern varying in frequency and time domains, where the three-dimensional distribution of energy is intermittent rather than continuous. This is because the transient energy is mainly determined by the frequency and amplitude of the waveform. The AE waveform information of coal and rock rupture is related to the released energy, which is mainly determined by the transient energy and duration. The three-dimensional energy spectrum more clearly shows the dynamic change characteristics of the MS waveform, reflecting the phase characteristics of the waveform, and each phase has its own frequency and energy characteristics. As shown in Fig. 5, at different stages of AE waveforms, the instantaneous energy varies significantly and has a distinct peak point. This is because the instantaneous energy is mainly determined by the frequency and amplitude. AE waveforms information of coal and rock rupture is related to the energy released and is mainly determined by the instantaneous energy and duration. By comparing the three-dimensional energy spectra, the peak energy points basically correspond to the peak amplitude points of the original signals. However, the peaks in the three-dimensional energy spectrum are more concentrated, the main peaks are more obvious and the main frequencies are significantly dominant. The instantaneous peak energies of the AE waveforms occur at the peak point of the waveform. This is due to the small amount of energy released during the initial stage of the coal and rock rupture. As the crack expands and energy builds up, the AE energy reaches a critical point at the peak of the waveform and is instantaneously released. By comparing the three-dimensional energy spectra, the peak energy points correspond to the peak amplitude points of the original time series signals. However, the three-dimensional energy spectra of the shale samples show large areas of energy distribution around the main peak, which indicates that the AE signals generated by the HF of the shale samples have more interference components, reflecting the difference in physical and mechanical properties between shale and other samples.

The decay characteristic of the AE signals is another important parameter in describing the waveforms, which reflects the process of convergence and dissipation of the waveform energy. To study the post-peak energy change characteristics of the AE signal induced by HF of coal and

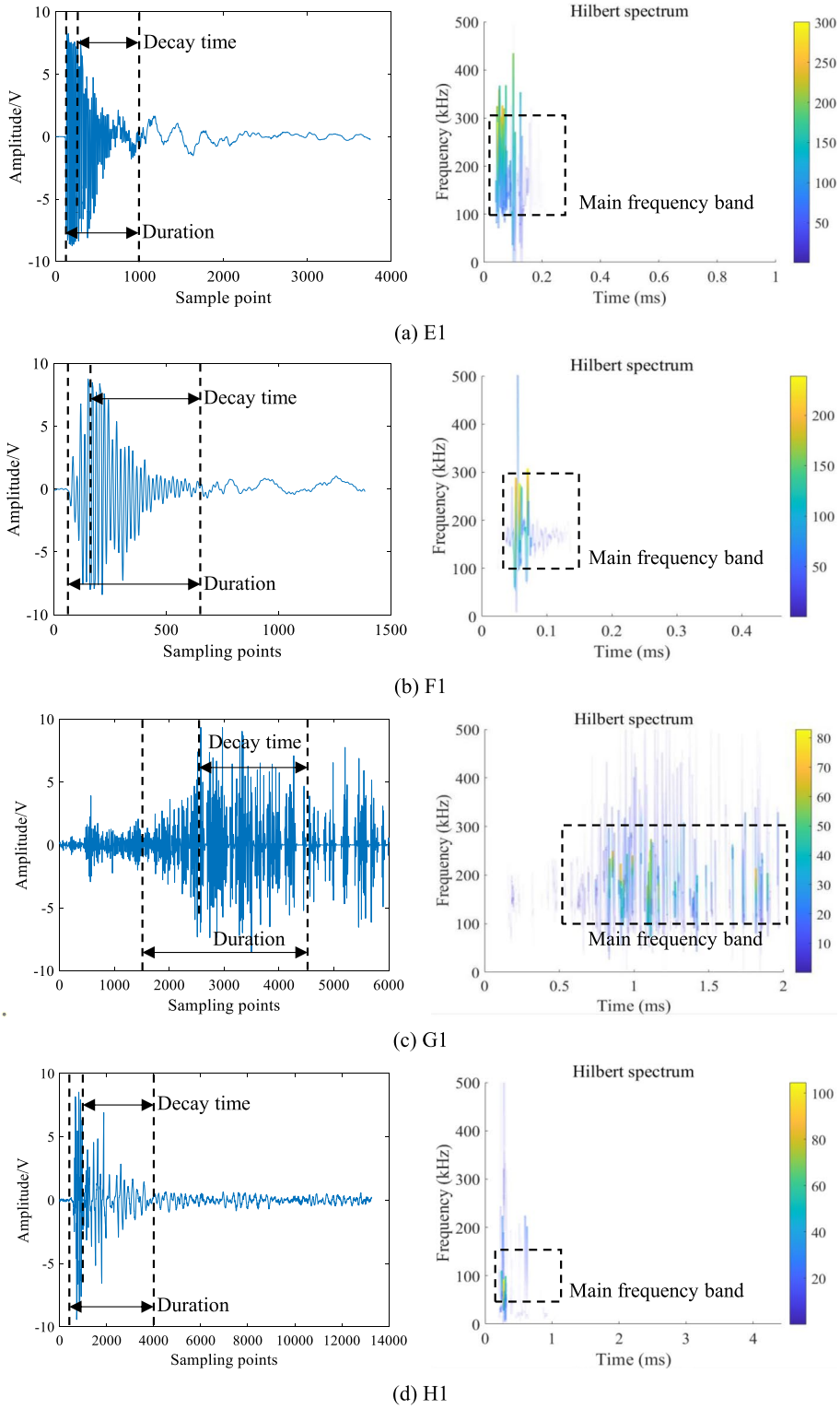

Fig. 4 AE waveforms and Hilbert spectra of different coal and rock HF

rock, the change process of the peak point down to the noise level point is defined as the decay process of the signal. The ratio of the post-peak decay time to the total duration of the waveform, known as the decay ratio, is used to quantify the decay process of the AE signals. The decay ratio of the AE signal can represent the decay characteristic of energy and thus reflect the effect of water participation on the HF and uniaxial compression signals. From Figs. 4 and 5, we can draw the following conclusions: From the time-energy perspective, the main energy of each IMF component of coal

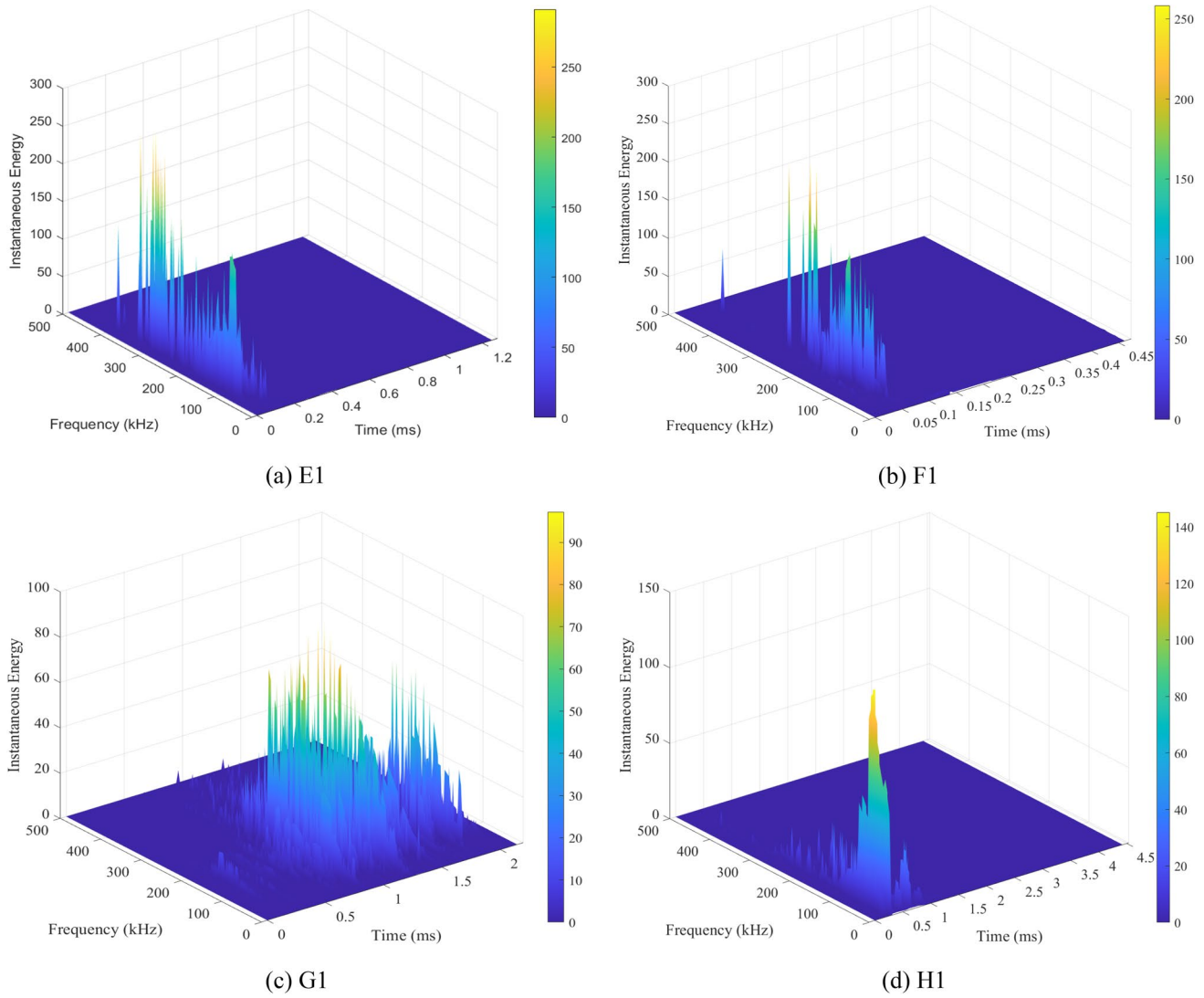

Fig. 5 Three-dimensional energy spectra of AE waveforms from different coal and rock HF

HF is mainly distributed between 100 and 1000 sampling points, that is, between 0.03 and 0.33 ms, with an approximate duration of 0.30 ms. The decay time is 0.23 ms, and the decay ratio is 0.78. The main energy of each IMF component of sandstone HF is mainly distributed between 100 and 700 sampling points, that is, between 0.03 and 0.23 ms, with an approximate duration of 0.2 ms. The decay time is 0.17 ms, and the decay ratio is 0.83. The main energy of each IMF component of shale HF is mainly distributed between 1500 and 4500 sampling points, that is, between 0.5 and 1.5 ms, with an approximate duration of 1 ms. The decay time is 0.67 ms, and the decay ratio is 0.67. The main energy of each IMF component of mudstone HF is mainly distributed between 500 and 4000 sampling points, that is, between 0.17 and 1.34 ms, with an approximate duration of 1.17 ms. The decay time is 1 ms, and the decay ratio is 0.85.

3.4 AE waveform characteristics of uniaxial compression waveforms

To study the effect of water on the AE signals of the HF, the characteristics of the AE signals under uniaxial compression conditions of the same coal and rock were analyzed. In the analysis of this paper, A1, B1, C1, and D1 were selected for analysis. The AE waveforms and Hilbert spectra of different coal and rock uniaxial compressions are shown in Fig. 6. As shown in Fig. 6, there was also a concentration of energy and frequency bands in the spectra of all four test samples. The main frequency band of the uniaxial compression of the coal sample was 150–350 kHz, that of the sandstone sample was 150–300 kHz, that of the shale sample was 100–300 kHz, and that of the mudstone sample was 200–350 kHz.

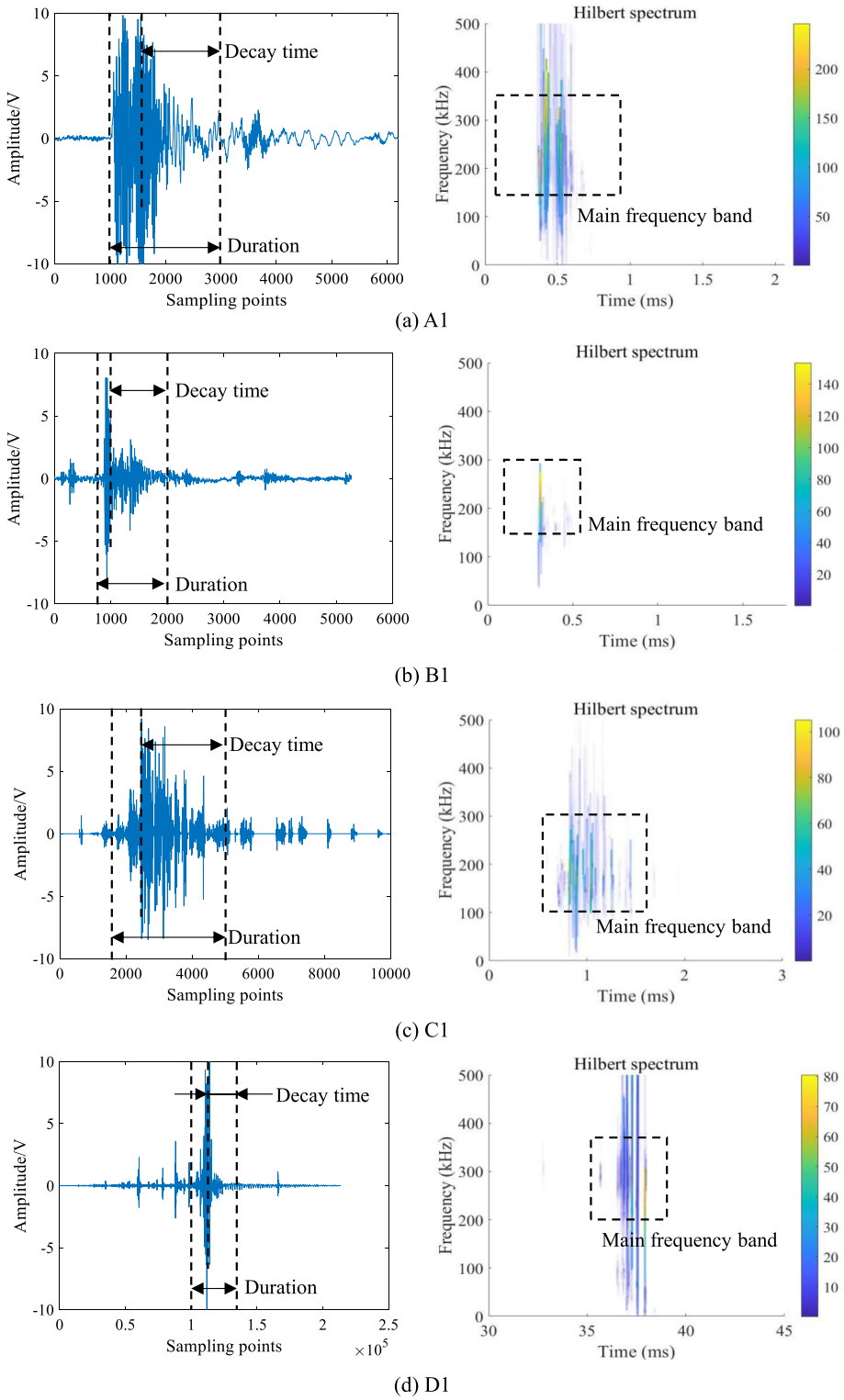

Fig. 6 AE waveforms and Hilbert spectra of different coal and rock uniaxial compression

A comparison of distribution of the main frequency bands of uniaxial compression and HF for different coal and rock samples is shown in Fig. 7. The main frequency bands corresponding to the AE waveforms of the shale sample did not change, which suggests that water had little effect on the shale samples. In contrast, the coal, sandstone, and mudstone samples showed varying degrees of reduction in the main frequency bands during the HF.

Three-dimensional energy spectra of the AE waveforms from different coal and rock uniaxial compressions

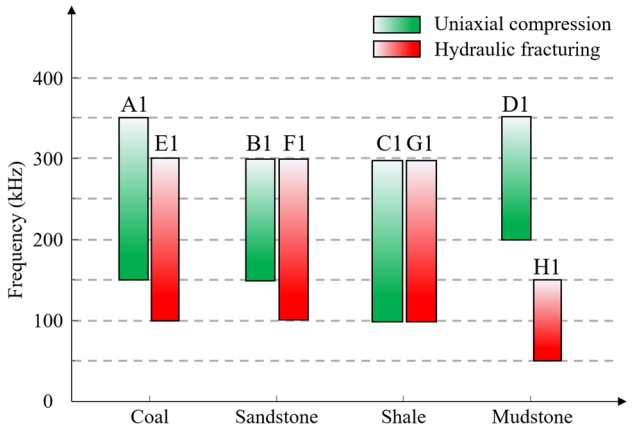

Fig. 7 Distribution of main frequency bands of different coal and rock sample rupture

are shown in Fig. 8. From Figs. 6 and 8, we can draw the following conclusions: From the time-energy perspective, the main energy of each IMF component of coal uniaxial compression is mainly distributed between 1000 and 3000 sampling points, that is, between 0.33 and 1 ms, with an approximate duration of 0.67 ms. The decay time is 0.50 ms, and the decay ratio is 0.75. The main energy of each IMF component of sandstone uniaxial compression is mainly distributed between 800 and 2000 sampling points, that is, between 0.27 and 0.67 ms, with an approximate duration of 0.4 ms. The decay time is 0.33 ms, and the decay ratio is 0.83. The main energy of each IMF component of shale uniaxial compression is mainly distributed between 1500 and 5000 sampling points, that is, between 0.50 and 1.67 ms, with an approximate duration of 1.17 ms. The decay time is 0.83 ms, and the decay ratio is 0.71. The main energy of

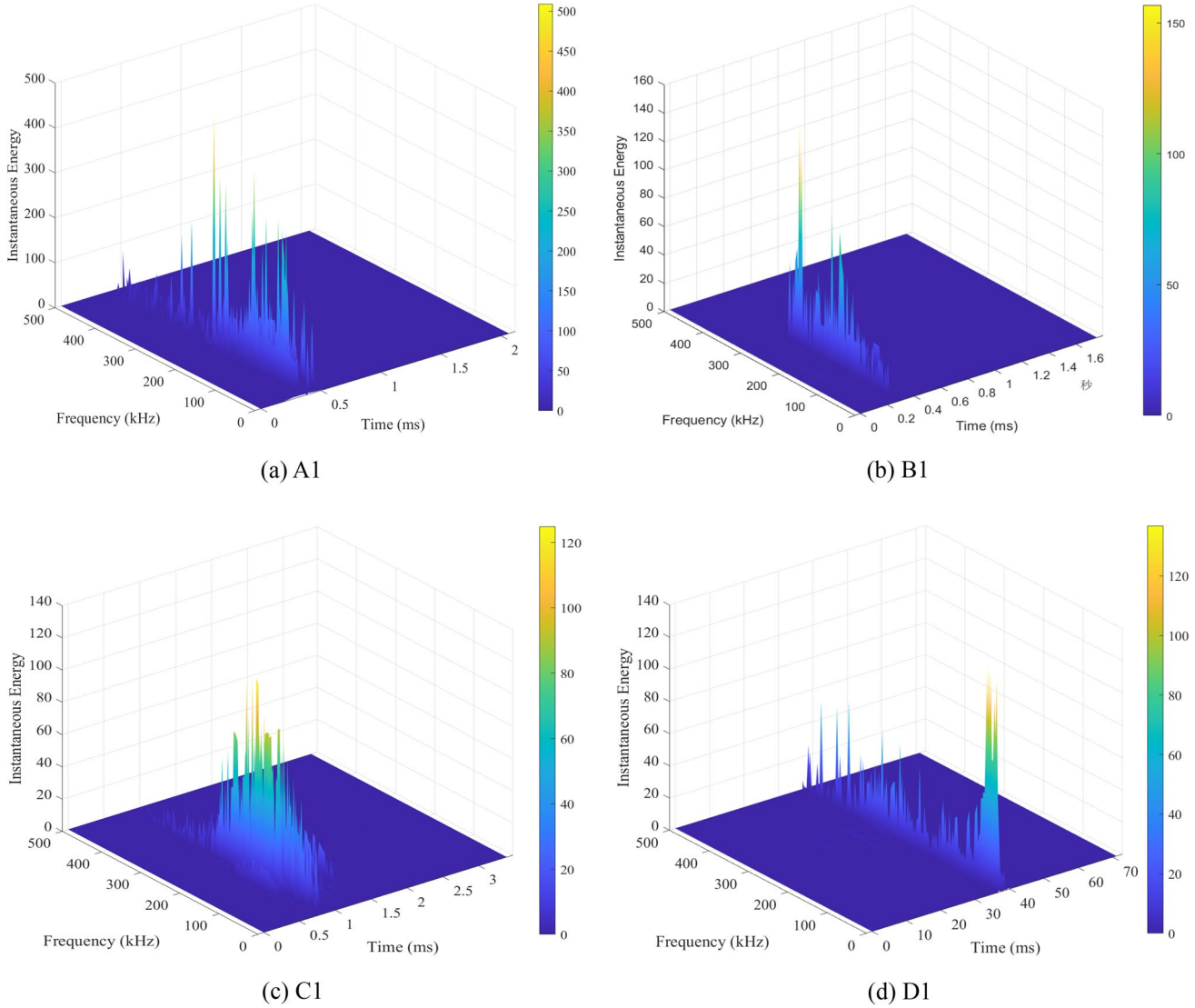

Fig. 8 Three-dimensional energy spectra of the AE waveforms from different coal and rock uniaxial compression

each IMF component of mudstone uniaxial compression is mainly distributed between 100,000 and 130,000 sampling points, that is, between 33.33 and 43.33 ms, with an approximate duration of 10 ms. The decay time is 6.67 ms, and the decay ratio is 0.67.

A comparison of the AE parameters of rupture of the different coal and rock samples is shown in Fig. 9. Although the amplitudes of the AE waveforms for uniaxial compression and HF are similar, the duration of the waveform during HF is significantly smaller than that of the uniaxial compression waveform; therefore, the energy carried by the HF waveforms is smaller. The longer the duration of coal and rock rupture, the higher the instantaneous and total energy. The decay ratio of the waveforms during HF was greater than that during uniaxial compression. The most significant differences in the decay ratios are observed for the mudstone samples. This indicates that the energy dissipation process of the AE waveforms was slower under the influence of water. The post-peak decay process becomes dominant over time, and the waveform energy exhibits a fast rise and slow fall. The stress levels and damage to the coal and rock can be estimated from the characteristics of instantaneous energy.

3.5 AE signal identification based on MLP

The transient time–frequency parameters of coal and rock rupture obtained by HHT provided a good indication of the characteristics of the samples. MLP neural network has high parallel processing capability and non-linear global action. It has good fault tolerance and associative memory function. The greatest function of MLP is that it can achieve nonlinear classification. Because the hidden layer is a fully connected layer, it can perform spatial transformation. A MLP neural network identification model based on the transient and AE monitoring parameters obtained by the HHT was proposed in this study. The identification process is illustrated in Fig. 10. A 4-layer MLP neural network model was constructed that included one input layer, two hidden layers, and one output layer. The input layer contained six neurons. The hidden layers had 64 neurons in each layer, and the ReLU was used as the activation function. The output layer had four neurons and used Softmax as the activation function. The maximum number of iterations of the MLP neural network was set to 3000. The weights and bias terms were initialized, and the back propagation (BP) algorithm was used to learn the weight parameters of the MLP neural network.

First, the AE monitoring parameters and transient parameters obtained by the HHT were extracted during HF and uniaxial compression process of coal, sandstone, shale, and mudstone samples. These include the amplitude, rise time, ringing count, instantaneous energy, centroid frequency, and instantaneous frequency. Different labels are assigned to different coal and rock rupture types. For HF signals, coal is "00", sandstone is "01", shale is "02" and mudstone is "03". For uniaxial compression signals, coal is "10", sandstone is "11", shale is "12", and mudstone is "13". Next, the training and validation sets of AE characteristic parameters for the rupture of the four coal and rock samples were input, as shown in Tables 2 and 3. There are 500 sets of training data for each lithology for a total of 2000 sets. There were 50 sets of validation data for each lithology for a total of 200 sets. Of these, HF and uniaxially compressed data are each split in half, and the label type for each training data is set in Table 2.

The MLP model was then trained iteratively, and the error term was calculated for each output unit. Finally, the BP algorithm is used to improve the weights and bias terms, as well as iterate and update the parameters. When the iteration ends, the minimum loss function values and identification results are outputted, as shown in Table 4. The lithological identification accuracy for the coal and sandstone samples

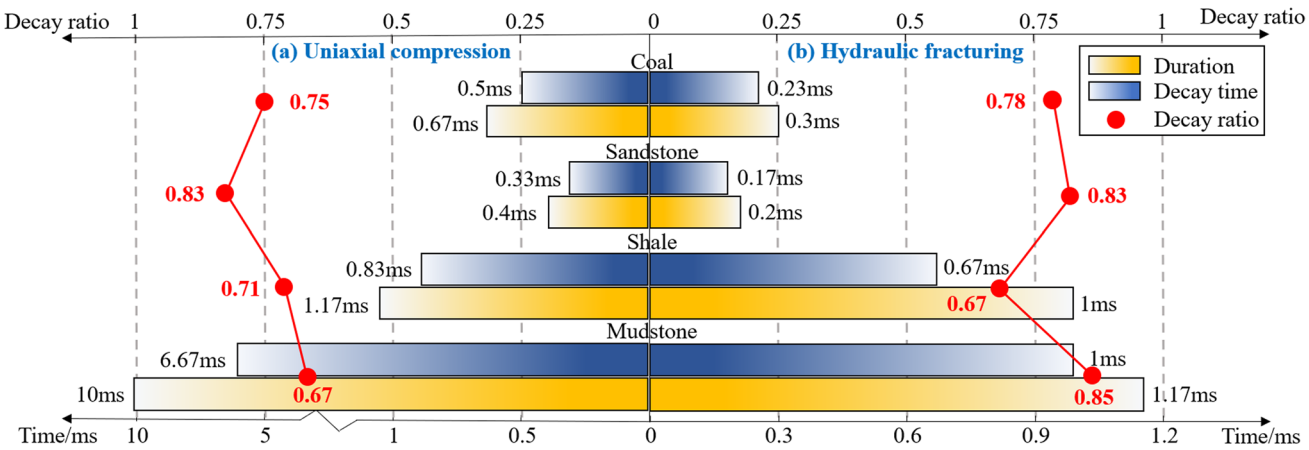

Fig. 9 Comparison of the AE parameters of different coal and rock sample rupture

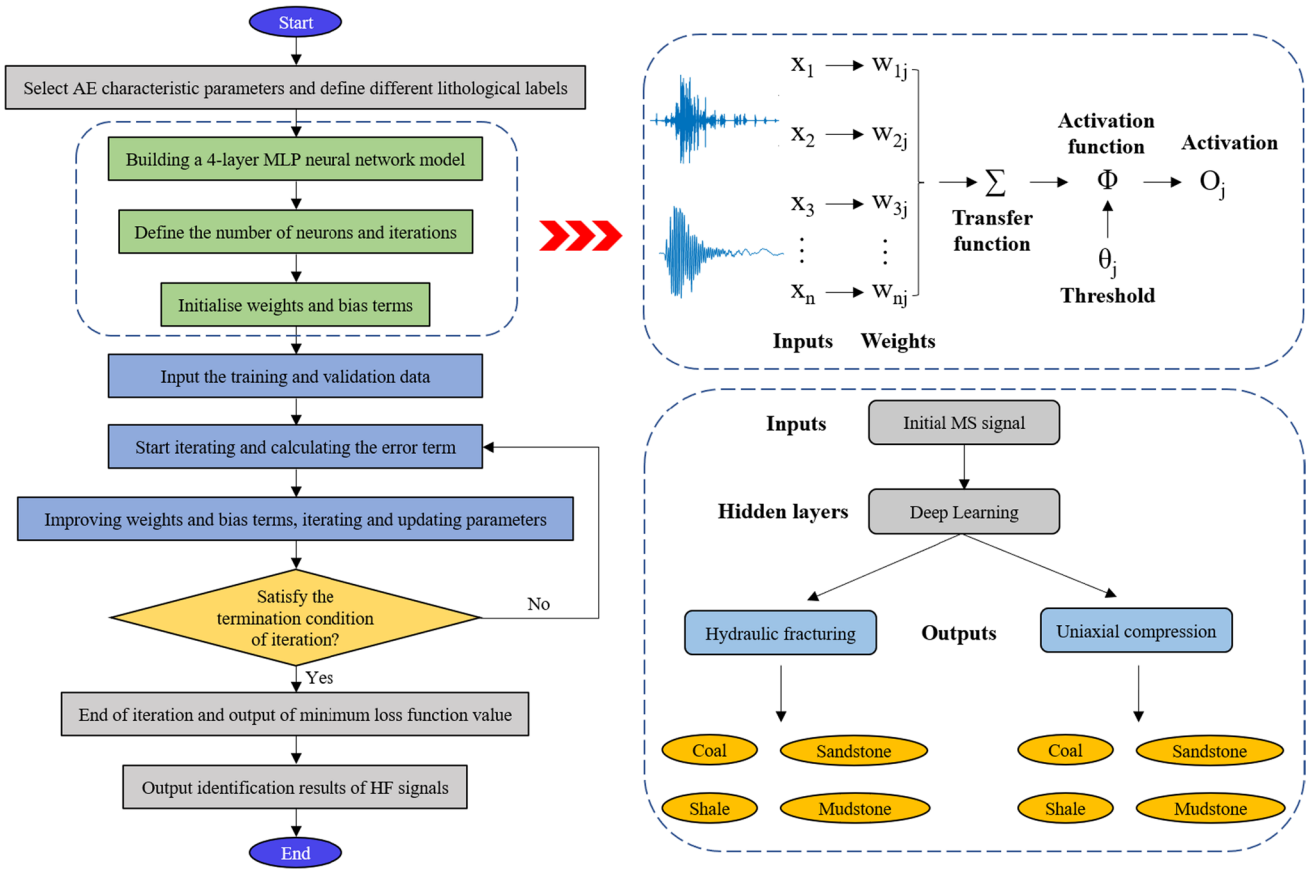

Fig. 10 Identification procedure of MS signals based on MLP neural network

Table 2 Training sets of AE signals during coal and rock HF

Number	Type	Amplitude (mV)	Rise time (μs)	Ringing count	Instantaneous energy	Centroid frequency (Hz)	Instantaneous frequency (Hz)
1	00	125.12	1.2512	19	5.59	203,099	164,062
2	00	37.84	0.3784	12	0.98	269,111	152,343
499	10	44.25	0.4425	10	1.9	236,338	128,906
500	10	71.72	0.7172	19	3.98	191,698	169,921
501	01	32.96	82.00	13	0.99	336,639	46875
502	01	38.45	82.00	15	1.2	319,456	23437
999	11	36.62	61.00	14	0.71	276,500	164,062
1000	11	32.65	20.00	12	0.29	388,296	93750
1001	02	560.3	17.33	14	20.23	256,751	93750
1002	02	142.21	6.67	18	6.03	310,311	93750
1499	12	113.83	0.33	10	74.48	214,778	167,724
1500	12	318.91	6.00	16	3.77	266,765	117,187
1501	03	122.07	1.33	12	1.29	392,121	187,500
1502	03	162.35	0.67	13	13.49	286,091	164,062
1999	13	111.69	0.33	18	27.18	120,798	8789
2000	13	118.71	2.00	12	14.93	221,264	14648

Table 3 Validation sets of AE signals during coal and rock HF

Number	Type	Amplitude (mV)	Rise time (μs)	Ringing count	Instantaneous energy	Centroid frequency (Hz)	Instantaneous frequency (Hz)
1		37.84	0.38	13	0.98	269,111	152,343
2		36.01	0.36	14	0.42	312,473	140,625
49		39.37	0.39	16	2.71	215,994	11718
50		41.81	0.42	16	7.21	172,148	5859
51		32.96	13.67	13	0.22	381,788	187,500
52		34.48	14.00	13	0.27	405,970	187,500
99		47.61	26.67	15	0.5	247,351	140,625
100		36.32	31.67	14	0.44	326,192	140,625
101		113.53	24.67	13	2.14	433,172	187,500
102		123.6	17.33	12	1.21	296,761	187,500
149		121.77	0.67	12	1.73	349,257	117,187
150		146.48	7.33	15	2.52	174,725	140,625
151		116.58	0.33	12	2.12	204,046	164,062
152		307.31	2.33	13	3.46	126,738	46875
199		137.02	2.67	12	1.74	240,436	46875
200		149.54	0.67	13	1.48	467,971	187,500

Table 4 Identification results of AE signals during coal and rock HF

Number	Type	Number	Lithology	Number	Lithology	Number	Lithology
1	00	51	01	101	02	151	02
2	00	52	01	102	03	152	03
3	00	53	01	103	02	153	03
4	00	54	01	104	02	154	03
5	00	55	01	105	03	155	03
6	00	56	01	106	02	156	02
7	00	57	01	107	02	157	03
8	00	58	01	108	02	158	03
43	10	93	11	143	13	193	13
44	10	94	11	144	12	194	13
45	10	95	11	145	12	195	13
46	10	96	11	146	12	196	13
47	10	97	11	147	12	197	13
48	10	98	11	148	12	198	13
49	10	99	11	149	12	199	13
50	10	100	11	150	12	200	13

was 100%, but a small amount of error occurred in the identification results for the shale and mudstone samples. This is owing to the influence of the physical properties of the samples and the electrostatic interference of the AE equipment during the experiment, resulting in an unstable AE signal, which led to incorrect identification results. During the experiment, it should be ensured that the laboratory equipment and instruments are well grounded to reduce the build-up of static electricity and interference. Ensure that the experimental process is in a quiet environment to reduce the influence of noise on the test results. Overall, the MLP neural network identification model achieved an accuracy of 96% for all four samples. The identification results validated the high accuracy and effectiveness of the MLP model.

4 Discussion

The overall direction of the experimental results showed that the differences in lithology lead to significant differences in AE signal characteristics. These changes in AE characteristics provide the basis for the identification of MS signals of

coal and rock ruptures. It also improves the ability to receive and process signals from small-scale, low-energy HF events. When the ruptured coal seam is thick and extensive, this method is effective in reducing the search area for locating the target rock layer. This improves the accuracy of the evaluation of the HF range and provides an effective guide for field operations of HF.

The mechanical properties and AE characteristics of coal and rock change after water immersion, which reflects the changes in the microstructure of the sample at the macroscopic level. It provides a basis for identifying and picking up effective HF events. The effect of water–rock interaction on the mechanical properties of rocks ranges from microstructural changes to macroscopic deterioration of physical properties (Wang et al. 2019). When the external or internal stress of rock reaches a certain level, the movement of crystalline interfaces at the microscopic level and the separation of mineral particles and slip of structural surfaces at the macroscopic level will occur. The characteristics of the AE signals during these processes are closely related to the rock rupture mechanism (Liu et al. 2020). The loss of intergranular cementing material within the rock under soaking conditions is severe. As a result, the microstructure becomes loose and the structural integrity decreases. The presence of water has a significant softening effect on the compressive strength of coal and rock samples (Guo et al. 2021). Softening of large granular minerals leads to a decrease in events such as microcrack compaction, microcrack sprouting, and frictional slip within the rock during sample damage, resulting in a reduction in AE energy (Kang et al. 2017). The test results confirm this hypothesis. The duration of the HF waveform was much shorter, resulting in less total energy.

Lithology is a comprehensive representation of various macro-physical and micro-physical and mechanical properties of different types of coal and rock. Owing to the variation in lithology, the dynamic rupture process and AE waveform characteristics of the coal and rock samples are different. Coal and rock masses have concentrations of various minerals, and different coal and rock masses have experienced different geological actions after their formation, making them different in composition and structural characteristics (Liu et al. 2018). Coal and rock samples with different structures and compositions exhibit different physical and mechanical properties. Coal is a sedimentary rock, but the different genetic materials and genetic environments between coal and other sedimentary rocks lead to large differences in properties between coal and rocks (Cheng and Pan 2020). Sandstone is a sedimentary rock with sand-based clasts that is generally rich in quartz grains and cemented between sand grains by authigenic minerals. Shale and mudstone are clay rocks that have poor water resistance, low strength, and tend to soften. As seen in Sect. 2.2, the UCS of the different coal and rock samples are shale, sandstone, mudstone, and coal in descending order, and the elastic moduli are sandstone, shale, mudstone, and coal in descending order. In general, the greater the structural surfaces of the rock, the greater the degree of compression damage, and the weaker the carrying capacity of the rock (Zhang and Zhao 2014).

The difference in porosity and hydrophilicity between coal and rock helps to further distinguish the AE signals of the HF and uniaxial compression. Coal and rock are composed of many mineral grains in the microstructure, and micropores and microcracks are widely distributed between mineral crystals. Generally, the porosity of coal is 2%–8%, that of sandstone is 1.6%–28.0%, that of shale is 0.4–10.0%, and that of mudstone is 3%–7%. Because water in rocks is stored in pores, the porosity and pore structure of the rock determine the magnitude of the water content of the rock (Li et al. 2016a, b). If the pore space is connected, the water in it has a significant influence on the AE characteristics of the rock damage. Otherwise, if the pores are disconnected, the effect (Zhou et al. 2017) is small. The hydrophilicity of different coals and rocks varies owing to differences in their hydrology. Different coals and rocks show very different properties after interaction with water during the HF test, including water content, water absorption, permeability, softening, swelling, and other characteristics. This is also helpful for identifying AE signals from different coal and rock HF and uniaxial compression.

5 Conclusions

(1) The AE energy and pumping pressure curves have a consistent variation. A decrease in pump pressure results in an increase in AE energy. The change in AE cumulative energy reflects the process of hydraulic fracture generation and expansion.

(2) After the EMD of AE waveforms for coal and rock rupture, the IMF1 component has the highest frequency and shortest fundamental wavelength. The energy of the AE waveforms was focused on IMF1–IMF3. The AE waveforms of different coal and rock rupture showed similar energy and frequency distribution characteristics after EMD.

(3) Concentrations of energy and frequency bands occurred in Hilbert spectra of different coal and rock HF. The main frequency bands of the coal, sandstone, and shale samples are 100–300 kHz, and the main frequency band of the mudstone sample HF is 50–150 kHz. The decay ratios of coal, sandstone, shale and mudstone samples are 0.78, 0.83, 0.67 and 0.85, respectively.

(4) By comparing with uniaxial compression waveform, the duration of the coal and rock HF waveforms is smaller, the transient and total energy carried is also

smaller, and the decay ratio is larger under the effect of water, with mudstone samples showing the most obvious performance.

(5) According to the training and identification of the AE monitoring parameters and transient parameters by the HHT and MLP neural networks, the accuracy of identifying different coal and rock HF and uniaxial compression signals was 96%.

Acknowledgements This paper was supported by the National Natural Science Foundation of China (52074049), Chongqing Natural Science Foundation (cstc2021jcyj-msxmX0764) and the Independent Research fund of The State Key Laboratory of Mining Response and Disaster Prevention and Control in Deep Coal Mines (Anhui University of Science and Technology) (SKLMRDPC19KF07).

Authors' contributions YQ: Data curation, Writing- Original draft preparation, Software. QL: Writing-Reviewing and Editing, Methodology. QH: Supervision. ZJ: Visualization, Investigation. RL: Writing- Reviewing and Editing. JL: Validation. WL: Software. CY: Investigation.

Availability of data and materials The data used in this study were obtained from the corresponding author, who can be contacted at liqg@cqu.edu.cn.

Declarations

Competing interest The authors declare that they have no known competing financial interests or personal relationships that could have appeared to influence the work reported in this paper.

References

Cheng Y, Pan Z (2020) Reservoir properties of chinese tectonic coal: a review. Fuel 260:116350

Damani A, Sondergeld CH, Rai CS (2018) Experimental investigation of in situ and injection fluid effect on hydraulic fracture mechanism using acoustic emission in Tennessee sandstone. J Pet Sci Eng 171:315–324

Guo P, Gu J, Su Y, Wang J, Ding Z (2021) Effect of cyclic wetting-drying on tensile mechanical behavior and microstructure of clay-bearing sandstone. Int J Coal Sci Technol 8(5):956–968

Huang NE, Shen Z, Long SR et al (1998) The empirical mode decomposition and the Hilbert spectrum for nonlinear and non-stationary time series analysis. P Roy Soc A-Math Phy 454(1971):903–995

Huang NE, Shen Z, Long SR (1999) A new view of nonlinear water waves: the Hilbert spectrum. Annu Rev Fluid Mech 31:417–457

Jiang Z, Li Q, Hu Q et al (2019) Underground microseismic monitoring of a hydraulic fracturing operation for CBM reservoirs in a coal mine. Energy Sci Eng 7(3):986–999

Jiang Z, Li Q, Hu Q et al (2020) Acoustic emission characteristics in hydraulic fracturing of stratified rocks: a laboratory study. Powder Technol 371:267–276

Kang Y, Yang B, Li X, Yang J, You L, Chen Q (2017) Quantitative characterization of micro forces in shale hydration and field applications. Pet Explor Dev 44(2):328–335

Kong X, Wang E, Hu S, Shen R, Li X, Zhan T (2016) Fractal characteristics and acoustic emission of coal containing methane in triaxial compression failure. J Appl Geophys 124:139–147

Li C, Liu J, Wang C, Li J, Zhang H (2012) Spectrum characteristics analysis of microseismic signals transmitting between coal bedding. Saf Sci 50(4SI):761–767

Li Q, Lin B, Zhai C (2015) A new technique for preventing and controlling coal and gas outburst hazard with pulse hydraulic fracturing: a case study in Yuwu coal mine, China. Nat Hazards 75(3):2931–2946

Li X, Li Z, Wang E et al (2016a) Extraction of microseismic waveforms characteristics prior to rock burst using Hilbert–Huang transform. Measurement 91:101–113

Li J, Li X, Wang X et al (2016b) Water distribution characteristic and effect on methane adsorption capacity in shale clay. Int J Coal Geol 159:135–154

Li N, Zhang S, Zou Y, Ma X, Wu S, Zhang Y (2018) Experimental analysis of hydraulic fracture growth and acoustic emission response in a layered formation. Rock Mech Rock Eng 51(4):1047–1062

Li D, Wang E, Kong X, Ali M, Wang D (2019) Mechanical behaviors and acoustic emission fractal characteristics of coal specimens with a pre-existing flaw of various inclinations under uniaxial compression. Int J Rock Mech Min 116:38–51

Li N, Li B, Chen D et al (2020) Waveform characteristics of earthquakes induced by hydraulic fracturing and mining activities: comparison with those of natural earthquakes. Nat Resour Res 29(6):3653–3674

Li N, Fang L, Sun W, Zhang X, Chen D (2021a) Evaluation of borehole hydraulic fracturing in coal seam using the microseismic monitoring method. Rock Mech Rock Eng 54(2):607–625

Li N, Sun W, Huang B, Chen D, Zhang S, Yan M (2021b) Acoustic emission source location monitoring of laboratory-scale hydraulic fracturing of coal under true triaxial stress. Nat Resour Res 30(3):2297–2315

Li Q, Qian Y, Hu Q et al (2022) Acoustic emission response mechanism of hydraulic fracturing in different coal and rock: a laboratory study. Rock Mech Rock Eng 55(8):4657–4672

Liang Y, Cheng Y, Zou Q, Wang W, Ma Y, Li Q (2017) Response characteristics of coal subjected to hydraulic fracturing: an evaluation based on real-time monitoring of borehole strain and acoustic emission. J Nat Gas Sci Eng 38:402–411

Liang Z, Xue R, Xu N, Li W (2020) Characterizing rockbursts and analysis on frequency-spectrum evolutionary law of rockburst precursor based on microseismic monitoring. Tunn Undergr Sp Technol 105:103564

Liu XS, Tan YL, Ning JG, Lu YW, Gu QH (2018) Mechanical properties and damage constitutive model of coal in coal-rock combined body. Int J Rock Mech Min 110:140–150

Liu Y, Yin G, Li M et al (2020) Mechanical properties and failure behavior of dry and water-saturated anisotropic coal under true-triaxial loading conditions. Rock Mech Rock Eng 53(11):4799–4818

Moriya H, Fujita T, Niitsuma H, Eisenblatter J, Manthei G (2006) Analysis of fracture propagation behavior using hydraulically

induced acoustic emissions in the bernburg salt mine, Germany. Int J Rock Mech Min 43(1):49–57

Mueller TM, Gurevich B, Lebedev M (2010) Seismic wave attenuation and dispersion resulting from wave-induced flow in porous rocks—a review. Geophysics 75(5):A147–A164

Niemz P, Dahm T, Milkereit C, Cesca S, Petersen G, Zang A (2021) Insights Into hydraulic fracture growth gained from a joint analysis of seismometer-derived tilt signals and acoustic emissions. J Geophys Res-Sol Ea 126:e2021JB02305712

Stanchits S, Burghardt J, Surdi A (2015) Hydraulic fracturing of heterogeneous rock monitored by acoustic emission. Rock Mech Rock Eng 48(6):2513–2527

Wang G, Jiang C, Shen J, Han D, Qin X (2019) Deformation and water transport behaviors study of heterogenous coal using CT-based 3D simulation. Int J Coal Geol 211:103204

Wang X, Hu Q, Li Q (2021) Investigation of the stress evolution under the effect of hydraulic fracturing in the application of coalbed methane recovery. Fuel 300:120930

Xiao P, Qian B, Jiang P, Xu N, Li B (2018) Deformation forecasting of surrounding rock mass based on correlation between frequency and fracture scale of microseismicity. Adv Civ Eng 2018:4037402

Yue Y, Peng S, Liu Y, Xu J (2019) Investigation of acoustic emission response and fracture morphology of rock hydraulic fracturing under true triaxial stress. Acta Geophys 67(4):1017–1024

Zhang QB, Zhao J (2014) A review of dynamic experimental techniques and mechanical behaviour of rock materials. Rock Mech Rock Eng 47(4):1411–1478

Zhang J, Peng W, Liu F, Zhang H, Li Z (2016) Monitoring rock failure processes using the hilbert-huang transform of acoustic emission signals. Rock Mech Rock Eng 49(2SI):427–442

Zhang X, Li Z, Niu Y, Cheng F, Ali M, Bacha S (2019a) An experimental study on the precursory characteristics of EP before sandstone failure based on critical slowing down. J Appl Geophys 170:103818

Zhang Z, Wang E, Zhang Y et al (2019b) Analysis on the time-frequency characteristics of ultrasonic waveform of coal under uniaxial loading. Fractals 27:19501006

Zhang B, Tian X, Ji B, Zhao J, Zhu Z, Yin S (2019c) Study on microseismic mechanism of hydro-fracture propagation in shale. J Pet Sci Eng 178:711–722

Zhou Z, Cai X, Chen L, Cao W, Zhao Y, Xiong C (2017) Influence of cyclic wetting and drying on physical and dynamic compressive properties of sandstone. Eng Geol 220:1–12

Zou Y, Zhang S, Zhou T, Zhou X, Guo T (2016) Experimental investigation into hydraulic fracture network propagation in gas shales using CT scanning technology. Rock Mech Rock Eng 49(1):33–45